The influence of flexible sound insulation layers on the seismic performance of cross laminated timber walls

Boris Azinović [*], Tomaž Pazlar , Meta Kržan

Section for Timber Structures, ZAG Ljubljana – the Slovenian National Building and Civil Engineering Institute, Ljubljana, Slovenia

A R T I C L E   I N F O

A B S T R A C T

This paper presents the results of an experimental campaign investigating the seismic behaviour of full-size cross laminated timber (CLT) wall systems with sound-insulated shear-tension angle brackets. The main aim of the study was to investigate the influence of more and less flexible soundproofing bedding under the CLT wall. The paper shows a comparison of lateral load-bearing capacity, displacement capacity, ductility and stiffness obtained from racking tests on uninsulated specimens and specimens with various types of bedding insulation and levels of vertical load. Moreover, an analytical procedure to estimate the lateral load-displacement response of CLT walls with bedding insulation is proposed. This model is verified by direct comparison to the experimentally determined lateral load-displacement backbone curves. The results show that the elastomeric bedding does not have a significant effect on the bearing capacity of the wall system tested, but it reduces the stiffness and increases the displacement capacity. Due to the large decrease in stiffness, the insulation causes an overall reduction in ductility. The analytical estimation proposed was able to capture the reduction in lateral stiffness and adequately predict the load-bearing capacity.

1. Introduction

As a result of the development of cross laminated timber (CLT), in recent years several high-rise and complex buildings have been constructed with load-bearing elements made of wood [1–3]. Since CLT structures offer many advantages, such as sustainability, energy efficiency, and rapid construction, they are also becoming more common in regions prone to earthquakes [4,5]. Ductile connections play a crucial role in achieving earthquake-resistant CLT structures by ensuring the deformation capacity and energy dissipation of the structural system. Besides the load bearing capacity and ductility, information on the connection stiffness is equally important to obtain realistic modal vibration periods of buildings for seismic design [6].

Sound insulation, and protection against unpleasant vibrations under service loads, are, due to the light weight of multi-story timber structures, also challenging aspects of design [7]. One of the ways to reduce disturbing sound transmission over flanking components is to use special elastic acoustic layers between the CLT wall and CLT floor panels [8]. The design of an appropriate elastic layer depends on the static loads to which the structural elements in the building and the insulation layer will be subjected, as well as their dynamic parameters, in order to

achieve good acoustic performance. Additionally, to prevent acoustic bridges via connectors, special sound-insulated steel angle brackets have recently been developed, in which the rigid parts are elastically separated from one another in order to prevent the transmission of sound [9, 10]. In contrast to traditional CLT connectors (hold-downs and angle brackets, e.g. Refs. [11,12]), the sound-insulated angle bracket solution achieves comparable tensile (up-lift) and shear strength by using additional inclined fully threaded screws [9]. This principle has also been adopted by other manufacturers of CLT connectors (e.g. Refs. [13,14]). Consequently, when the CLT wall panel is loaded laterally, such connections are subjected to both shear and tension/compression loading. In previous studies, it has been found that the coupling effect in CLT connections should not be neglected in numerical models for design [15–17], so the connections should therefore be tested for bi-axial loading. In addition to the bi-axial testing of individual connections, an even more appropriate method for simulating combined loading is the cyclic testing of CLT wall systems, which can be used to investigate the kinematic behaviour of single or multiple wall systems. In order to further understanding of the behaviour of the bedding insulation and the insulated angle bracket connector developed with respect to the response of the CLT structural system under seismic loading, the racking

---

tests presented in this paper were performed on full-scale CLT wall specimens following preceding cyclic tests on a single angle bracket [9].

The racking CLT wall experiments are performed to better understand the mechanical behaviour of CLT wall panels under in-plane lateral loading, and can also serve as a basis for determining numerical models or analytical equations that can be used to predict the lateral response of CLT structures (e.g. caused by wind or seismic actions). In recent years, based on racking experiments, Gavrić et al. [18] have developed advanced analytical models for nonlinear pushover analysis of CLT wall systems, which take into account all the stiffness and strength components of the connections, as well as the bending and shear deformation of the panels. A parametric study of CLT wall systems carried out to compare the influence of different wall aspect ratios and segmentation on the response, showed that the segmentation of CLT walls reduces their stiffness and strength, but significantly improves their deformation capacity. In Refs. [19–22], suitable equations were presented to describe the elastic and elastoplastic behaviour of a single-story CLT shear wall and CLT walls arranged in series (multi-panel CLT shear walls). The proposed models can be used to determine the internal distribution of forces on panels and connections, as well as the elastic or elastoplastic force-displacement curves for the various possible kinematic cases (Coupled-Panel and Single-Wall kinematic behaviours). Elastoplastic analytical methods for multi-panel CLT shear walls were investigated by sensitivity analysis to consider the effect of the contribution from the biaxial behaviour of the angle brackets and hold-downs [22]. The results of the sensitivity analysis showed that, by accounting for the biaxial behaviour of the connections, more panels maintained contact with the ground, leading to lower displacement and rotation. Several other investigations have been carried out based on CLT shear wall experiments with the aim of improving numerical modelling approaches (e.g. Refs. [23–31]) and the design of CLT buildings (e.g. Refs. [32–36]). Additionally, in Ref. [37], the influence of timber perpendicular-to-the-grain compression properties on the overall seismic behaviour of CLT walls was investigated by means of numerical analyses, and a general analytical model was proposed to schematize the wall-to-slab and wall-to-foundation connections. It was found that the inclusion of timber compressed parallel-to-the-grain did not significantly influence the initial elastic stiffness of the CLT structure (before uplifting of the vertical panels), but when seismic action increased the stiffness decreased significantly, breaking down the maximal base shear force.

The research presented had two main objectives; firstly, to experimentally evaluate the structural performance of a CLT wall system with soundproofing details (soundproofing bedding and insulated angle brackets), since, to the authors' knowledge, no studies on the seismic performance of CLT panels with soundproofing layers have been published to date, other than the two tests conducted by Hummel et al. [38]; and secondly, to propose an addition to the existing analytical equations representing the CLT shear wall response, by including the contribution made by the deformable bedding insulation. In contrast to the study by Hummel et al. [38], which included tests on CLT walls connected with hold-downs and angle brackets, the present work used novel (insulated) angle brackets, which serve to prevent both shear sliding and uplift. In Ref. [38], a comparison of results between the CLT wall systems with and without bedding insulation revealed that the initial shear stiffness was about 60% lower in the insulated system compared to its uninsulated counterpart.

In this paper, the influence of the soundproofing details on the in-plane shear behaviour was investigated by conducting racking experiments on single-panel CLT walls. The influence of three different factors was analysed in this study: the type of soundproofing bedding below the CLT panel (differing in stiffness and static load limit), the level of vertical compression loads (varying from 10 to 100 kN/m), and the position of the insulated angle bracket (with respect to its distance from the edge of the panel). The experimental results were evaluated and compared to the analytical results obtained from the proposed analytical model,

which was upgraded in relation to previous studies to include the contribution of the bedding insulation.

2. Materials and methods

2.1. Test specimens and materials

The specimens were constructed from a 2490/2490/100 mm 3-layer (30-40-30 mm) CLT wall panel connected to a 3150/500/140 mm 5-layer (40-20-20-20-40 mm) CLT slab by two $100 \times 100 \times 3$ mm steel angle brackets with additional 14 mm thick metal plates over the horizontal legs [9]. CLT without narrow edge bonding was used, with a board strength of class C24 (ETA 14–0349 [39]), an average density of 467 kg/m^3 and a moisture content of 10.4%–12.8%, as measured during testing. The aim of the experimental program was to obtain results regarding the cyclic behaviour of the insulated angle brackets for use in CLT walls. The outer laminations were therefore arranged orthogonally to the CLT slab, which is the most common orientation in CLT walls. The angle brackets were placed on one side of the wall panel only (Fig. 1). They were fastened to the wall panel with 8 fully threaded 8×80 mm screws (ETA 11–0284 [40]), and to the slab with 10 fully threaded 8×160 mm screws (ETA 11–0284 [40]) - 4 installed vertically in the middle section of the steel plate, and 3 on each side at an angle of 45° in order to achieve a higher withdrawal capacity. The type and configuration of the screws were determined by the angle bracket manufacturer, with the capacity design principle not explicitly considered. It has already been shown that different failure mechanisms occur under tensile loading in such angle bracket connections (withdrawal of the screws from the floor panel, embedment of the screws in the wall panel, etc.) [9]. For actual use in seismic regions, the capacity design principle should be applied such that the failure mechanism in the predefined part of the connection is more controlled.

To investigate the influence of the bedding insulation on the lateral response, two different groups (four types) of insulation material were placed under the walls, according to the level of vertical load applied; moderately flexible insulation (labelled SR55 and NB) for low level vertical loads (10 kN/m), and stiffer insulation (labelled SR1200 and NF) for higher levels of vertical load (50 kN/m) [41]. The two different groups of insulation sheet differed in cellular structure (mixed vs. closed-cell polyurethane structure) and consequently, according to the manufacturer, in their nonlinear behaviour under cyclic loading. Despite each having a different influence on sound insulation (mixed-cell elastomers are characterised by highly elastic behaviour, while closed-cell elastomers offer better sound damping), similar mechanical behaviour was expected under static and low-cycle dynamic loading. The type of insulation placed under the wall was determined based on its effectiveness in terms of preventing sound transmission, as a function of the static compressive stresses to which the wall and insulation layer would be subjected. For the insulated walls, a 12.5 mm layer of bedding insulation was laid under the wall (Fig. 1). The angle brackets, on the other hand, were always insulated with the same sound insulation (moderately flexible, closed-cell polyurethane, labelled NC), which was placed in two layers (one under the flange and one between the flange and the metal plate) to a total thickness of 12.5 mm (Fig. 1). The distance of the angle brackets from the edge of the walls (b_e) was 150 mm for the first series of tests. As, following the tests, the CLT panels were only damaged locally, at the location of the connections, the same CLT panels were then further used for the second set of tests with a b_e equal to 400 mm.

2.2. Testing program

The testing program (Table 1) consisted of 11 shear tests varying in terms of the presence and type of insulation (stiff or flexible), in the application of vertical load, and in the distance of the angle brackets from the edges of the CLT wall. To determine the amplitude
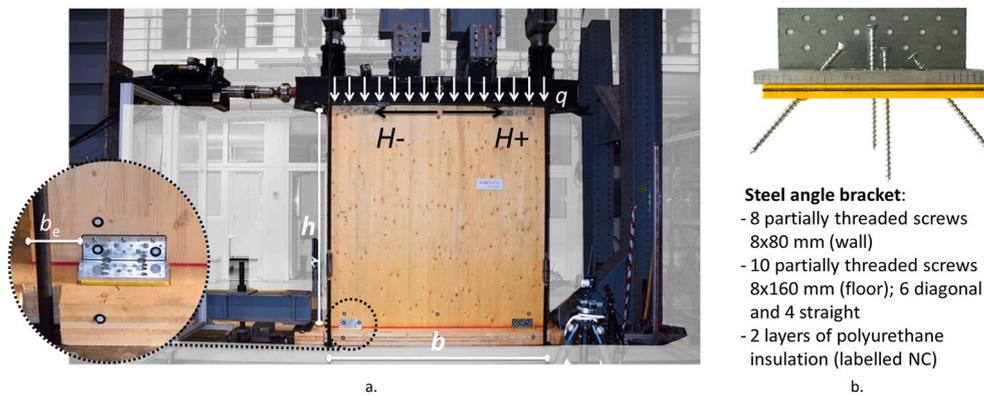
Fig. 1. a. Test setup with basic denotations, and b. description of the angle bracket connection used for all test specimens.

Table 1
Racking tests conducted on CLT walls, varying in terms of insulation type, the distance of angle brackets from the edge of the wall, and the level of vertical load.

Test	Type	Vertical load [kN/m]	Loading rate [mm/s]	Edge distance b_e [mm]	Soundproofing bedding
W-Unin/15-M/1	Monotonic	10	0.5	150	none
W-Unin/15-C/1	Cyclic	10	0.5	150	none
W-Unin/15-C/2	Cyclic	100	0.5	150	none
W-SR55/15-C/1	Cyclic	10	0.5	150	SR55 (Flex.Ins.)
W-NB/15-C/1	Cyclic	10	0.5	150	NB (Flex.Ins.)
W-SR1200/15-C/1	Cyclic	50	0.5	150	SR1200 (Stiff.Ins.)
W–NF/15-C/1	Cyclic	50	0.5	150	NF (Stiff.Ins.)
W-NB/15-C/2	Cyclic	50	5.0	150	NB (Flex.Ins.)
W-Unin/40-C/1	Cyclic	10	0.5	400	none
W-SR1200/40-C/1	Cyclic	50	0.5	400	SR1200 (Stiff.Ins.)
W-SR55/40-C/1	Cyclic	10	0.5	400	SR55 (Flex.Ins.)

displacements of the loading cycles, a preliminary monotonic test was conducted on an uninsulated wall, using the same test setup as the cyclic tests (presented in Fig. 1).

The tests' boundary conditions were designed to represent a real case scenario equivalent to an actual CLT building; vertical load was applied to the wall by two hydraulic actuators at levels of 10, 50 and 100 kN/m and was kept constant during the test. The load was applied to the top of the wall panel through a steel box beam, enabling uniform distribution of the lateral and vertical loads. Out-of-plane displacements of the specimens were restrained by steel angle brackets positioned at the top of the wall panel, while movement of the steel box beam was also laterally restrained by a steel element with a PTFE layer in order to eliminate friction (Fig. 1).

Horizontal loading was applied using a servo-hydraulic actuator with a capacity of 250 kN and controlled through lateral displacement at the top of the panel. A loading rate of 0.5 mm/s was applied in all tests except W-NB/15-C/2, since a very slow loading rate (0.02–0.2 mm/s) is defined in EN 12512. This is in accordance with the standard for testing timber connections ISO 16670:2003 [42], where a loading rate range of 0.1–10 mm/s is prescribed. The amplitude of the loading protocol adopted in all cyclic tests was based on the results of the yield displacement capacity, as obtained from monotonic tests on an uninsulated wall specimen. The loading was induced in cycles by subsequently increasing the displacement amplitude from the initial position in both directions. The increase in displacement amplitude was determined according to EN 12512 [43] as a definite part of yield displacement d_y. After the first two cycles of increasing the displacement amplitude the loading protocol consisted of three cycles at each displacement amplitude in order to obtain the strength and stiffness degradation [43].

The vertical force induced by two actuators was measured with two load cells placed below the actuators (on top of the steel beam), and was kept constant during the test, simultaneously controlled by the load cells. The test was displacement controlled by inducing lateral

displacement at the top and centre point of the CLT wall panel, as measured by a 200-mm linear variable displacement transformer (LVDT). The relative horizontal displacement at the bottom (between the wall and the floor panel) was measured by a 100-mm LVDT positioned at the centre of the panel. The relative vertical displacements were measured by 100-mm LVDTs at each end of the CLT wall panel. Additionally, the displacements were measured at 16 discrete points using a professional digital image correlation system. The points of measurement were positioned on the CLT wall, the CLT slab, the angle brackets and on the steel beam through which the loading was induced.

2.3. Input data for the analytical estimation

Three basic material components were considered in the mechanics-based analytical prediction model proposed in this study: (i) CLT, (ii) sound-insulated angle brackets, and (iii) soundproofing bedding. As shown in Fig. 1, the CLT wall has overall dimensions of b x h x a and is subjected to a horizontal force, H, and a uniformly distributed vertical load, q. Since the damage to CLT panels under shear loading is concentrated in the connections, it was assumed that the CLT wall elements behave elastically. The in-plane shear stiffness of the panel was calculated considering the shear modulus of the CLT panel defined in Ref. [39] i.e. the shear modulus of CLT G_{eff} was assumed to be 0.46 GPa. Alternatively, in-plane shear stiffness could be calculated considering the shear modulus of the structural timber used for individual laminations (class C24 in the present study) and the gross cross section of the CLT with a shear correction factor, as defined in previous studies [44, 45]. Only vertical laminations were considered for the elastic bending stiffness of the CLT wall, with an assumed elastic modulus of 12 GPa [39]. In the compression zone of the CLT slab, the elastoplastic behaviour of CLT was assumed using an elastic modulus perpendicular to the fibre ($E_{90,mean}$) of 0.37 GPa [39], compressive strength perpendicular to the fibre ($f_{c,90}$) of 3.0 MPa (according to Ref. [46]), the factor $k_{c,90}$ equal to 2.0 (considering the load configuration and the degree of compressive

deformation), and an elastic limit strain ($\varepsilon_{90,el}$) of 0.75%, as proposed in Ref. [37].

The actual cyclic response of the innovative sound insulated angle bracket connections was investigated in a previous study, where detailed information and results can be found [9]. For the analytical approach presented in this study, their mechanical behaviour is described by tri-linear force-displacement relationships in both the shear and tensile directions (Table 2). The points in the tri-linear relationship, defined as the mean values from multiple tests on the innovative connections, and from the mean backbone curve derived from positive and negative directions of loading, are summarised in Table 2. The elastic response is represented by the elastic stiffness ($k_{con,el}$), which is calculated as secant stiffness between 10% and 40% of the load-bearing capacity of the connection ($F_{con,max}$). When the force exceeds 40% ·$F_{con,max}$, a reduced stiffness $k_{con,pl,1}$ is applied, which is calculated as the secant stiffness between 40% and 90% $F_{con,max}$. The descending branch of the trilinear relationship, from $F_{con,max}$ until the ultimate displacement of the connections ($u_{con,u}$), is described by the equation $k_{con,pl,2} = 0.5 \cdot k_{con,pl,1}$. This tri-linear approximation provides a simple but relatively accurate description of the connections in terms of the accuracy of results from the analytical model regarding the behaviour of CLT shear walls.

To investigate the influence of the insulation, tests were carried out on walls containing two groups of bedding insulation, differing in elastic properties and static load limit: (i) a stiffer insulation with a static load limit of up to 1.5 MPa (NF and SR1200, referred to as "Stiff.ins.", used in structures for higher static loading) and (ii) a moderately flexible type of insulation with a static load limit of about 0.05 MPa (NB and SR55, referred to as "Flex.ins.", used for lower static loading, e.g. in the upper floors of structures).

Fig. 2 shows compressive deformation under static loading in the 12.5 mm thick insulation, considering a shape factor of 3.0 for strip bedding (a geometric measure of the shape of the bedding, defined as the ratio of the loaded area to the area of the sum of the perimeter surfaces [41]). The Flex.ins. bedding is strongly inelastic under compressive stress (<3 MPa), while the Stiff.ins. primarily stays in an elastic state. The corresponding deformation reaches up to 80% of the initial thickness (12.5 mm) in the Flex.ins., compared to up to 25% of the initial thickness in the Stiff.ins. In non-seismic areas, the design requires only the elastic diagram, since the bedding insulation is primarily compressed by the presumed static vertical load in a uniform fashion, so there is little possibility for higher stresses (e.g. due to a rocking mechanism). In order to calculate the rotation of the wall due to lateral seismic loads and the consequent unequal vertical displacements of the bedding insulation, full stress-strain diagrams of the bedding insulation are required (Fig. 2). The present study considers the exact compressive displacements of the insulation (from diagrams), corresponding to compressive stress at the wall corner, evaluated at discrete critical points of the analytical lateral load-displacement curves.

Additionally, the shear deformation of the bedding insulation also proved to have an effect on the total displacement at the top of the wall. A linear elastic response was considered in the shear direction, with the
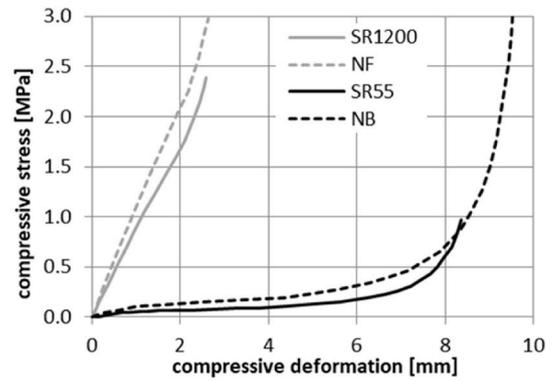

Fig. 2. Compressive displacement of the 12.5 mm thick bedding insulation under static load for Flex.ins. and Stiff.ins. [41].

shear modulus of the insulation (G_{ins}) being about 30% of its elastic modulus (in compression) for Flex.ins., and 10% for Stiff.ins.

3. Description of the analytical estimation model

Besides its geometrical characteristics and vertical load, the kinematic behaviour of CLT wall systems under lateral loads mainly depends on the anchoring connections (e.g. angle brackets or hold-downs), and, in multi-panel shear walls, the vertical joints screwed between adjacent CLT wall elements (not investigated in this paper). The total top displacement (δ) of a single CLT wall element can be derived as the sum of the following components [Eq. (1)]: rocking (δ_r), sliding (δ_{sl}), shear deformation of CLT (δ_{sh}) and bending deformation of CLT (δ_b) [18]. In the case of CLT walls, the lateral deformation of walls due to a deformable foundation could also be considered as part of the rocking displacement δ_r. In the present study, however, the contributions of the deformable bedding insulation (δ_{ins}) and the CLT slab (δ_{com}) are added separately to the total displacement δ, since this way the contribution of the insulation itself, its stiffness, and the contribution of the CLT slab are more straightforward. Furthermore, the contribution δ_{ins} also includes the shear deformation of the bedding insulation. It should be noted that in actual multi-storey platform-type CLT structures other contributions to the total top displacement are present, such as the top rotation of the CLT wall in the storey below.

$$\delta = \delta_r + \delta_{sl} + \delta_{sh} + \delta_b + \delta_{com} + \delta_{ins} \tag{1}$$

The equations used in this paper for the kinematic behaviour of the CLT wall are similar to those used in the studies by Gavrić et al. [18] and Casagrande et al. [19]. The principle of the multi-linear curve in the
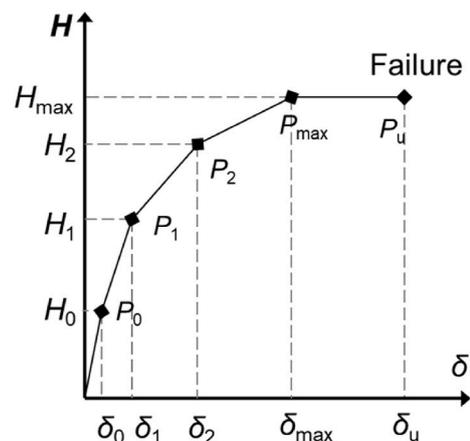
Table 2
Assumed points of the tri-linear force-displacement curve with respect to the shear and tensile behaviour of the connections, based on average test results [9].

	Shear	Tensile	Force-displacement diagram
$k_{con,el}$ [kN/mm]	4.18	4.07	
$k_{con,pl,1}$ [kN/mm]	2.13	2.47	
$F_{con,el}$ [kN]	31.8	21.5	
$F_{con,max}$ [kN]	79.6	53.8	
$u_{con,max}$ [mm]	28.8	18.0	
$u_{con,u}$ [mm]	43.1	27.3	

Fig. 3. General definition of the multi-linear diagram for the shear response of CLT walls.

general inelastic diagram of the CLT shear wall response (Fig. 3), and the bi-axial behaviour of the mechanical anchors were considered, as by Masroor et al. [22], while the concept of including the (in)elastic compressive deformation of the CLT slab is similar to that considered by Sandoli et al. [37], which was further adapted to include the (in)elastic compressive deformation of the insulation. In the general multi-linear response diagram shown in Fig. 3, the point P_0 represents the stage when the compressive deformation at the uplift side of the CLT panel reaches zero, P_1 the stage when the rocking mechanism is activated, P_2 is achieved when the first critical connection starts to yield, P_{max} when the bi-linear criterion for the maximum strength of the critical connection is satisfied (the state of other angle brackets is checked and their stiffness adapted accordingly), and P_u when the bi-linear criterion for the maximum displacement of the critical connection is reached.

3.1. Rocking behaviour

In the case of single wall behaviour (Fig. 4), the lateral deformation on top of the wall due to rocking (δ_r) is derived from the moment equilibrium at the point of rotation (PoR):

$$\delta_r = \frac{\left(H \cdot h - \frac{q \cdot b^2 (2\beta - 1)}{2}\right) h}{\sum k_{con,y,i} \cdot x_i^2} \quad (2)$$

where H is the total lateral force at the top of the CLT wall (depending on the stage; H_0, H_1, H_2, H_{max}), h is the height of the CLT wall, b is the width of the CLT wall, q is the uniformly distributed vertical load, $k_{con,y,i}$ is the stiffness of each connection in the tensile direction (depending on the internal forces in the connection and their inelastic diagram, $k_{con,el}$, $k_{con,}$

$_{pl,1}$ or $k_{con,pl,2}$, x_i are the distances from the PoR to the centre of connection), and β is the influence of the compression zone.

Previous experimental investigations of CLT shear walls (e.g., Refs. [22,35]) have shown that the PoR of the wall is not located at the corner of the panel. This is due to the compressive deformation in the CLT slab or in the CLT wall (in the case of a stiff foundation), which causes a compressive zone. When the compressive zone is highly deformed, the PoR moves further towards the centre of the panel, meaning the distance to the connection on the uplift side (x_i) is reduced. This effect is incorporated in the proposed model by assuming a reduced panel length equal to $\beta \cdot b$. The influence of the bedding insulation on the PoR and rocking behaviour was considered separately in this study and is included in δ_{ins}. For the rocking mechanism the PoR is assumed to be at the centre of the compressive zone. The length of the compressive zone (x_{com}) and coefficient β, which define the PoR, are given by the equations:

$$x_{com} = \frac{q \cdot b}{a_{eff} \cdot k_{c,90} \cdot f_{c,90}} \quad (3)$$

$$\beta = \frac{b - x_{com}}{b} \quad (4)$$

where a_{eff} is the thickness of the compressed layer (thickness of the CLT wall), $k_{c,90}$ is a factor taking into account the load configuration, the splitting potential, and the degree of compressive deformation, and $f_{c,90}$ is the compressive strength perpendicular to the fibre (design, characteristic or mean value, depending on the purpose of the estimation).

In the case that the foundation under the panel is stiff, the rocking PoR would be defined by the length of the compressive zone in the CLT wall panel.
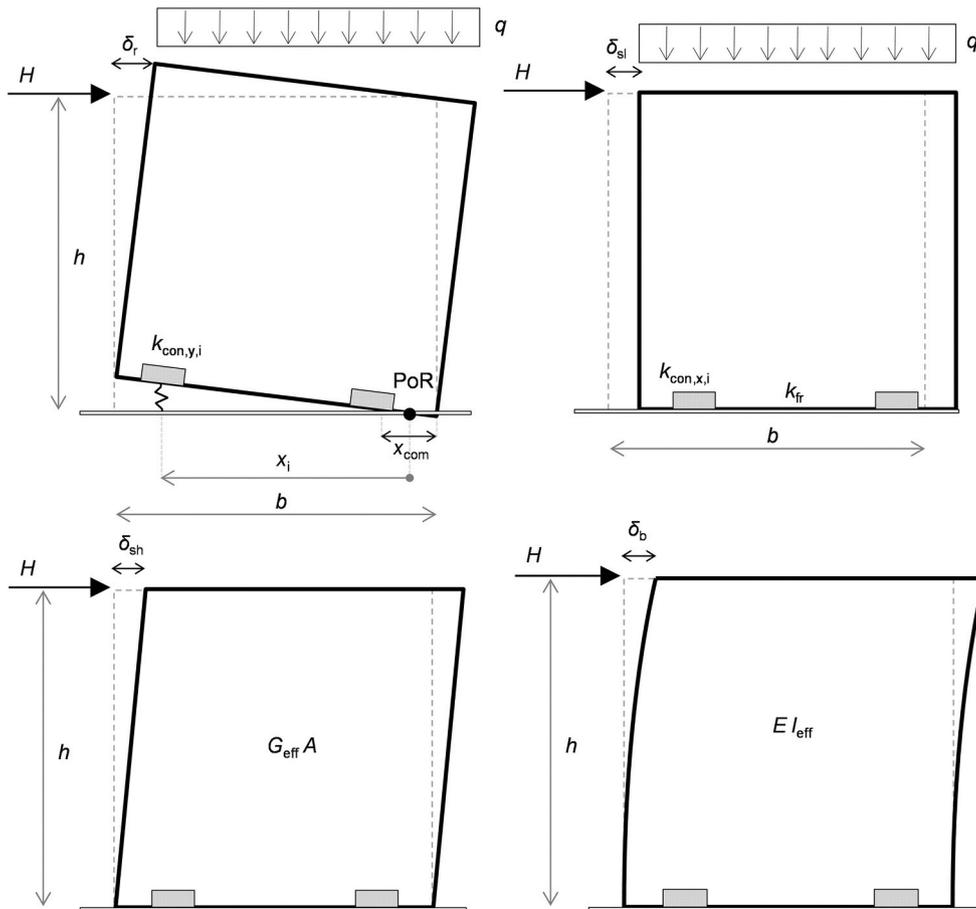

Fig. 4. Schematic showing the deflection components of a single CLT wall panel: rocking (δ_r), sliding (δ_{sl}), shear (δ_{sh}), bending (δ_b).

3.2. Sliding behaviour

The sliding deformation of a CLT wall system (δ_{sl}) is derived from the equilibrium of forces in the horizontal direction:

$$\delta_{sl} = \frac{H - k_{fr} \cdot q \cdot b}{\sum k_{con,x,i}} \tag{5}$$

where k_{fr} is the coefficient of friction between the CLT wall and the base, and $k_{con,x,i}$ is the stiffness of each connection in the shear direction – $k_{con,el}$, $k_{con,pl,1}$ or $k_{con,pl,2}$, depending on the stage in the inelastic diagram.

Sliding in the CLT systems starts when the total horizontal force, H, exceeds the static friction force ($k_{fr} \cdot q \cdot b$). This is a simplified estimation, since in reality the combined behaviour of rocking and sliding is more complex. The approach, however, proved to be sufficient for the purposes of this study. The coefficient of friction between the CLT wall and the slab (k_{fr}) was assumed to be 0.5 for both the insulated and uninsulated specimens, as determined by previous experiments of kinetic friction [9]. The coefficient is within the range of values found in the literature [47], although the results vary considerably with respect to different timber characteristics and are also dependent on the test setup. In the present study, the difference between static friction (which occurs prior to sliding) and kinetic friction was neglected, since in the study by Almeida et al. [48] relatively small differences between the coefficients of sawn timber under intermediate and high compression loads were found (on average static friction was 6% higher), and, without experimental tests, the uncertainty in friction coefficients is very high.

3.3. Shear and bending deformation of the CLT panel

As found in previous studies, the CLT wall panels generally remain in an elastic state; the shear deflection can therefore be calculated using the following equation:

$$\delta_{sh} = \frac{1.2 \, H \cdot h}{G_{eff} \cdot A} \tag{6}$$

where $G_{eff} \cdot A$ is the shear stiffness of the panel, G_{eff} the shear modulus of CLT and A the gross cross section of the panel.

The bending deflection on the top of the panel (δ_b) can also be calculated using the elastic formula:

$$\delta_b = \frac{H \cdot h^3}{3E \cdot I_{eff}} \tag{7}$$

where $E \cdot I_{eff}$ is the flexural stiffness of the CLT panel, with the moment of inertia, I_{eff}, calculated by considering the vertical laminations of the CLT panel and the elastic modulus of the structural timber boards, E (strength class C24 in the present study).

3.4. Compression of the elastomer insulation and the CLT slab

The compressive forces at the contact surface between the CLT wall and the horizontal elements are resisted by timber-to-timber contact in the uninsulated wall specimens, and additionally by the insulation in the insulated panels. The contribution of the angle brackets to the compressive resistance was neglected in this model. The insulated angle brackets, however, are the only component in the system that can resist tensile forces. At the point of contact the cross section is loaded by a combined axial force and bending moment, divided by the neutral axis into sides of compression and tension (Fig. 5, stage 2). The CLT slab and/or the insulation reach their ultimate strain at the compressed corner, while the tensile resistant elements are in an elastic or inelastic state (yielded), depending on the position of the neutral axis.

Four different stages can be defined to describe the contact behaviour, depending on the position of the neutral axis (Fig. 5):
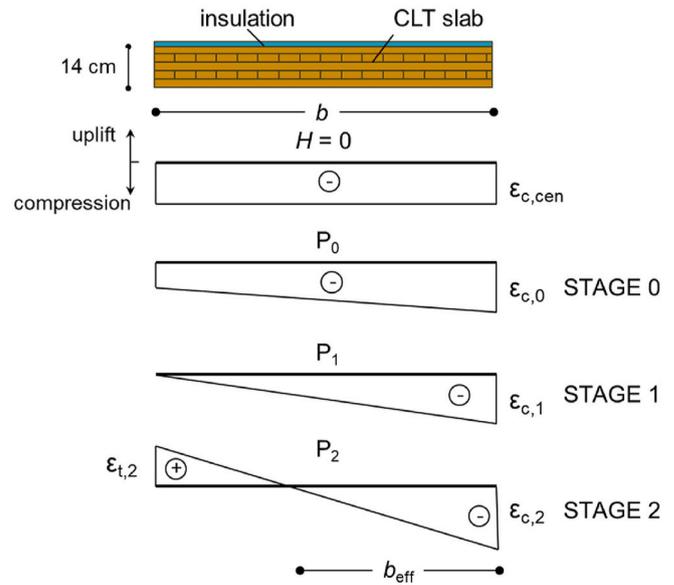

Fig. 5. Strain diagrams at the contact area below the CLT wall at different stages: from the centric compression stage (vertical force only) to the rocking stage.

(i) Centric compression, where the vertical load is uniform and thus centric compression is present - both the bedding insulation and the CLT slab should be designed to remain in the elastic state.

(ii) Stage 0, where a horizontal force is present, but is not high enough to overcome the total vertical loads and cause uplift on the tension side - in most mid-rise CLT buildings (<5 stories) the increase in compressive stress at this stage would not cause plasticity in either the CLT slab or the Stiff.ins. In the case of the Flex.ins., however, which behaves in a highly non-linear manner, this increase could cause residual deformation at the corner. To determine P_0 for the inelastic diagram, a critical shear force, H_0, was calculated [Eq. (8)], which causes the compressive stress at the corner of the uplift side to reach zero.

$$H_0 = \frac{q \cdot b^2}{6h} \tag{8}$$

(iii) Stage 1, where the horizontal force causes uplift of the panel from the contact area - tensile-resistant elements (angle brackets) are activated but remain in the elastic state. In contrast, depending on the material used and the boundary conditions, the bedding insulation and CLT slab may either behave elastically or may have already exceeded the strength of their elastic limit at the corner. To determine P_1 for the inelastic diagram, a critical shear force, H_1, was calculated using the moment equilibrium at the centre of the compression zone, as given by Eq. (9):

$$H_1 = \frac{q \cdot b^2 (2\beta - 1)}{2h} \tag{9}$$

(iv) Stage 2, where the horizontal force causes yielding of the angle bracket at the uplift side. The yielding of the angle bracket is caused by a combination of vertical and horizontal forces in the connection – the bilinear interaction is considered in the model, as described further in the paper. On the compression side, the CLT slab and the insulation can be in either the elastic or the inelastic state. The shear force in the CLT wall is increased until the bilinear criterion for the maximum force in the angle bracket is reached - either the uplift (tension) or the shear force is

predominant. The criteria to determine H_2 and H_{max} (critical horizontal loads) are given in the following section.

At each stage the compressive deformation (ε_c) of the thick bedding insulation at the compressed corner was determined, depending on the nonlinear diagram for the insulation material (Fig. 2), and the corresponding compressive stress:

$$\sigma_c = \frac{q}{a} - H \cdot \frac{6 \cdot h}{b^2 \cdot a} \qquad (10)$$

where σ_c is the compressive stress at the wall corner, and H is the total horizontal force acting on the panel (H_0, H_1 or H_2).

Similarly, the compressive deformation of the CLT slab was included in the estimation, where the linear-elastic law was adopted and the elastic moduli $E_{90,mean}$ was used in the calculation.

In systems with highly deformable insulation materials, the experiments proved that the shear deformation of the bedding insulation cannot be neglected when calculating the total top shear displacement of the wall. The shear deformation in the insulation, considering the total horizontal force H in all stages, was calculated using the following equation:

$$\gamma_{ins} = \frac{1.2 \cdot H}{G_{ins} \cdot a \cdot b_{eff}} \qquad (11)$$

where γ_{ins} is the average shear stress in the compressed part of the bedding insulation, G_{ins} is the shear modulus of the insulation, and b_{eff} is the length of the insulation under compression.

At each stage, when calculating the shear displacement (from the shear deformation γ_{ins}), the effective average thickness of the compressed bedding insulation ($t_{ins,eff}$) was considered. A simplification was assumed, whereby $t_{ins,eff}$ was calculated as the mean value of the insulation thickness at the compressed corner and the thickness at the position of the neutral axis.

The contribution of the compressive deformation of the CLT slab (δ_{com}) to the top shear displacement of the CLT wall (δ_{tot}) is determined by basic trigonometric functions, with the assumption made that the CLT panel rotates as a rigid body. The contribution of the compressive deformation of the bedding insulation was determined in the same way. The contribution of the insulation (δ_{ins}) to δ_{tot} includes both the compressive and shear deformation of the bedding insulation.

3.5. Strength capacity and the shear-uplift interaction of connections

Various prediction models for lateral resistance in CLT walls have already been proposed by several authors (e.g. Refs. [18,21,37]). Due to two-directional loading at the position of the innovative angle bracket, a reduction in the strength capacity should be taken into account. One possibility is to use the shear-uplift interaction inequality, where a linear or nonlinear working domain could be applied. In this study a nonlinear domain was used, given by the following equations:

$$\left(\frac{F_{con,x}}{F_{con,el,x}}\right)^2 + \left(\frac{F_{con,y}}{F_{con,el,y}}\right)^2 = 1 \qquad (12)$$

$$\left(\frac{u_{con,x}}{u_{con,max,x}}\right)^2 + \left(\frac{u_{con,y}}{u_{con,max,y}}\right)^2 = 1 \qquad (13)$$

where $F_{con,x}$ and $F_{con,y}$ represent the shear and uplift forces in the angle bracket considered and $F_{con,el,x}$ and $F_{con,el,y}$ the elastic limit strength of the connections in the shear and uplift directions, $u_{con,x}$ and $u_{con,y}$ the shear displacement and uplift calculated at the position of the angle bracket considered, and $u_{con,max,x}$ and $u_{con,max,y}$ the experimentally determined shear and uplift displacements corresponding to the maximum force value ($F_{con,max}$) in each direction.

In almost all cases, the critical connection, where the limit state first

occurs, is the connection closest to the uplift corner of the CLT wall. On rare occasions, in walls of the dimensions tested, it could occur that the shear mechanism of the wall would be predominant and a connection at any other position would prove critical. This would be possible in cases with high vertical load, or if connections varying in shear stiffness and capacity were used on the same wall (e.g. hold-down and angle brackets).

It was assumed that, once the limit condition expressed by Eq. (12) is attained (stage P_2), the plasticization of the connection would apply simultaneously in both directions (shear and uplift). The same condition was used to determine the stage P_{max}, where a displacement criterion was instead adopted (Eq. (13)). The distribution of the uplift forces, which is needed to determine the connection forces, was based on the stiffness ratio of the connections used and the distance of the connection from the PoR. Since the same angle brackets (of equal stiffness) were used on both sides, a triangular distribution of the uplift forces was assumed, where both connections are in an elastic state. On the other hand, the total shear force was distributed to each connection proportionally, according to the shear stiffness of the connections – depending on the state of the connection $k_{con,el}$ or $k_{con,pl}$. To determine stage P_u, a similar condition as in Eq. (13) was used, only the displacements at the maximum connection force were replaced by the ultimate displacements of the connection in each direction (as given by the experimental trilinear envelope described in Table 2). The limit shear forces for each stage (H_1, H_2, H_{max}) were determined by a numerical solver tool, using the conditions from Eqs. (12) and (13) and analytical equations for top shear displacement (Eq. (2)–(7)). Friction between the CLT walls and base was also considered in order to determine the limit stages.
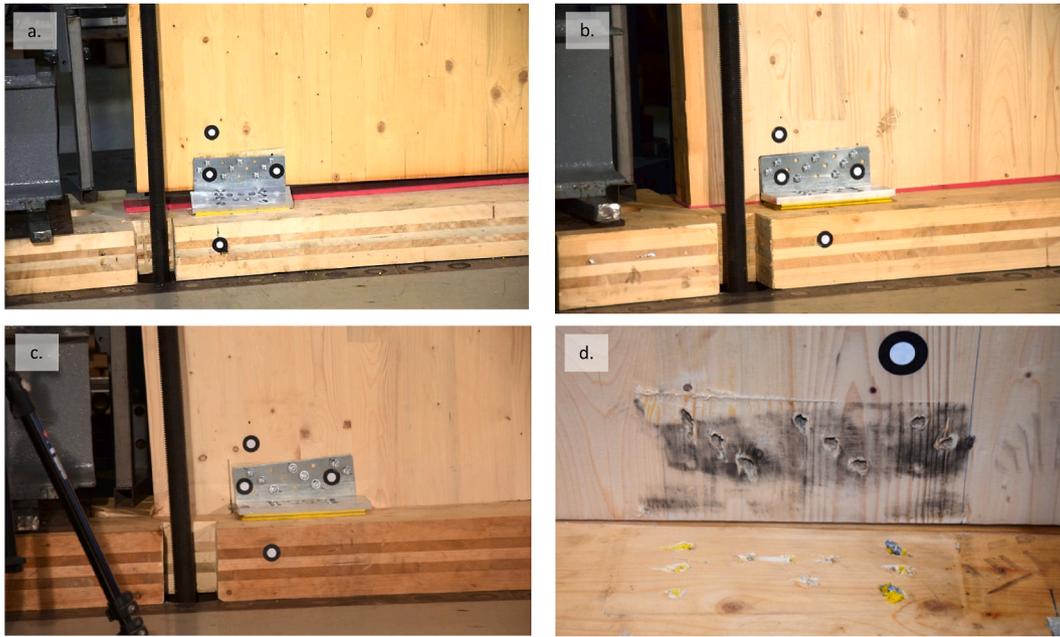
4. Results

4.1. Results of experimental tests

Different damage mechanisms occurred in the tests; in the first phases of the tests shear sliding occurred at the base of the wall. With rocking (up-lift) of the wall, large deformations were observed in the angle bracket, with withdrawal of the screws from the CLT slab (Fig. 6a) and embedding of the screws in the CLT wall panel (Fig. 6d). Since the load-bearing capacities of both parts of the connection (i.e. both the wall and slab parts of the connection) are similar under tensile (uplift) loading [9], no systematic rule was found to determine which of the two uplift mechanisms was more prevailing under any specific influencing parameter (i.e. the presence or type of insulation, level of vertical load or position of the angle brackets). Under higher vertical loads compression of the CLT slab under the CLT panel was evident (Fig. 6c), with minor compression also observed under the angle bracket (Fig. 6d). At the corner of the wall high deformation of the Flex.ins occurred, including in the specimens subjected to low vertical load (Fig. 6b). It should be noted that for high lateral loads the CLT foundation slab lifted from the ground, however, this did not influence the result significantly.

The influence of various parameters on the load-bearing and displacement capacity obtained, as well as other characteristics, is evident from comparisons of the experimental hysteretic lateral force-displacement curves, as presented in Fig. 7. Table 3 presents the average results for all tests in both directions of loading in terms of lateral displacements and resistances for the following characteristic performance limit points:

- the yield displacement, δ_y, and resistance H_y, defined according to EN 12512 [43] (the intersection of the backbone hysteretic curve between 10% and 40% H_{max} [elastic stiffness k_{el}, corresponding lateral displacements $\delta_{10\%}$ and $\delta_{40\%}$] and the tangent curve to the hysteresis envelope, assuming an inclination, k_{pl}, of $1/6 * k_{el}$),
- the maximum lateral load-bearing capacity, H_{max} [kN], and corresponding lateral displacement, δ_{Hmax} [mm],

Fig. 6. Damage mechanisms: a) plastic deformations of the angle bracket and withdrawal of the screws from the CLT slab, b) embedment of the soundproofing bedding, c) embedment of the CLT slab (uninsulated specimen) and d) embedment of the angle bracket into the slab and the screws into the CLT wall in experiments with the greatest vertical loading.

- the ultimate lateral displacement of the wall, δ_u (the displacement at which a 20% drop in the post-peak resistance was obtained, or the maximum displacement obtained if such a decrease in load was not obtained), and the corresponding lateral resistance in the first loading cycle, H_u.

Furthermore, Table 3 presents the ductility, μ, defined according to EN 12512 as the ratio of the ultimate displacement to the yield displacement. To be able to comprehensively compare the experimental response to analytical results, however, secant stiffness $k_{40\text{-}90}$ at 40% and 90% of H_{max}, and the potential (input) energy E_{INP} (area under the backbone curve) are presented, up to ultimate displacement.

One of the parameters that can only be obtained by cyclic tests is energy dissipation. Relative energy dissipation can be evaluated through the equivalent viscous damping coefficient v_{eq}, which was calculated according to EN 12512 for each loading cycle, with Table 3 presenting the average values of the third loading cycles for each test conducted.

In the monotonic test the values in Table 3 refer to only one direction of loading. It must be noted that the 20% drop in load-bearing resistance was not achieved in the first amplitude loading cycle in all tests due to limitations of the equipment (it exceeded the maximum displacement of the test set-up). For the same reason, in a few cases the load-bearing capacity was not achieved in either direction of loading (W-Unin/15-C/2, W-SR55/15-C/1, W–NF/15-C/1, W-SR55/40-C/1).

Denotations: $\delta_{10\%}$ and $\delta_{40\%}$ … lateral displacements on top of the wall corresponding to 10% and 40% H_{max}; k_{el} … secant stiffness between 10% and 40% H_{max}; $k_{40\text{-}90}$ … secant stiffness between 40% and 90% H_{max}; H_y … yield resistance defined according to EN 12512, with k_{el} and the tangent curve to the hysteresis envelope at an inclination of $1/6$ k_{el}; δ_y … yield displacement corresponding to H_y; H_{max} … the maximum lateral load-bearing capacity; δ_{Hmax} … displacement corresponding to H_{max}; H_u … ultimate resistance of the wall corresponding to δ_u; δ_u … ultimate lateral displacement of the wall defined according to EN12512; μ … ductility defined as the ratio δ_u/δ_y; E_{INP} … potential (input) energy.

Note: In tests W-Unin/15-C/2, W-SR55/15-C/1, W–NF-15-C/1, W-SR55/40-C/1 the load-bearing capacity was not achieved in either direction. In tests W-NB/15-C/1, W-Unin/40-C/1, W-SR1200/40-C/1 and W-NB/15-C/2 the 20% drop in load-bearing capacity was not obtained

in the first loading cycle.

4.2. Analytical model results

Analytical lateral load-displacement curves were calculated for all of the CLT wall systems tested, varying by insulation stiffness, vertical loading and angle-bracket position. In Fig. 8 some tests (uninsulated walls and wall systems with different types of insulation (Stiff.ins and Flex.ins), under different vertical loading with an angle bracket edge distance equal to 150 mm) are directly compared to the corresponding experimentally obtained backbone curves for the first loading direction.

The total lateral displacements (δ_{tot}) evaluated at limit points P_o-P_{max} (as described in Section 3) are presented for all CLT walls in Fig. 9. In order to compare the contributions of different mechanisms for the various wall systems, and to demonstrate the significance of each contribution in different phases of the response, the contributions of individual components to the total displacements are depicted in different colours. Lateral load resistances are also stated for the limit points in each wall system.

5. Discussion of results on the analysed walls

5.1. Validation of the analytical model

While a comparison of analytical results to experimental results in the first (positive) loading direction is presented in Fig. 8, Table 4 provides a comparison of the analytically estimated results with the average experimental results for each test in both directions of loading, as well as the average of the relative differences between them (the analytical curves were analysed in the same manner as the experimental ones). The error of analytically-estimated load-bearing capacity compared to results from various cyclic experimental tests is lower than 10% in all cases, i.e. the ratio of analytical to experimental H_{max} ranged between 0.91 and 1.03 (on average the analytical H_{max} was underestimated by 2%, with a 5% coefficient of variation (CV), not considering the monotonic test). The estimation of elastic stiffness, k_{el}, proved less accurate, leading to an average overestimation of 21%, with significantly higher scatter (23% CV). The larger difference and scatter can be
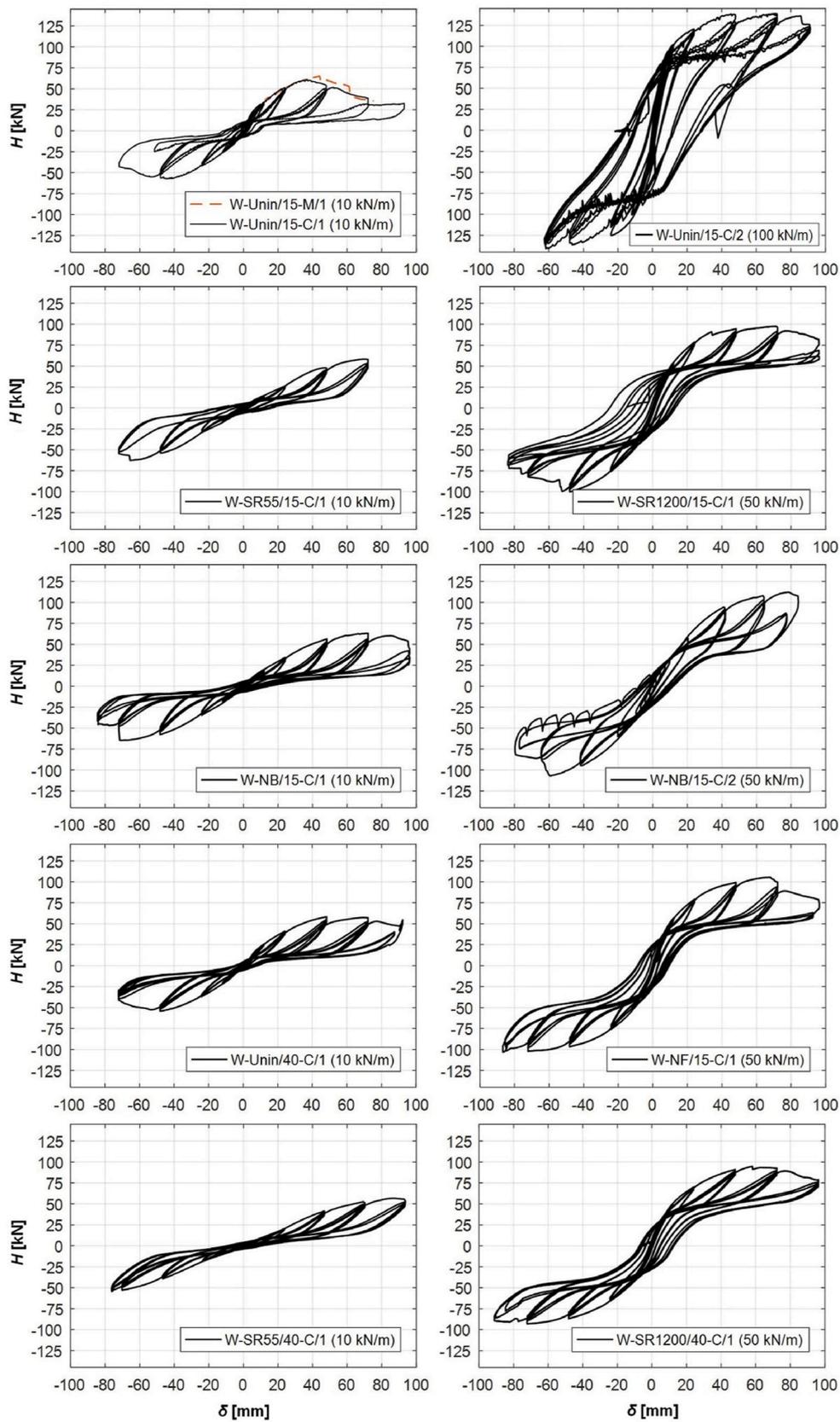
Fig. 7. Comparisons of the hysteretic lateral force-displacement response.

Table 3
Results of experimental tests on the walls (average results of both loading directions).

Test	$\delta_{10\%}$ [mm]	$\delta_{40\%}$ [mm]	k_{el} [kN/mm]	$k_{40\text{-}90}$ [kN/mm]	H_y [kN]	δ_y [mm]	H_{max} [kN]	δ_{Hmax} [mm]	H_u [kN]	δ_u [mm]	μ [/]	ν_{eq} [%]	E_{INP} [kNmm]
W-Unin/15-M/1	1.95	7.1	3.83	1.27	45.9	12.2	65.4	44.0	52.3	61.2	5.00		2940
W-Unin/15-C/1	1.80	7.8	3.11	1.20	45.8	15.7	58.9	40.8	47.1	62.0	4.25	7.0	2695
W-Unin/15-C/2	0.84	4.0	13.7	2.85	88.9	6.4	140.1	66.7	128.4	76.4	12.3	9.0	9188
W-SR55/15-C/1	3.55	20.7	1.06	0.88	57.9	52.4	60.6	67.6	48.4	72.0	1.37	7.3	2650
W-NB/15-C/1	2.87	16.6	1.39	0.97	56.2	38.6	63.9	71.5	51.1	85.5	2.22	5.7	3803
W-SR1200/15-C/1	1.51	7.9	4.68	1.63	73.8	15.4	99.0	59.5	79.2	84.6	5.72	5.4	6557
W–NF/15-C/1	1.44	8.0	4.81	1.47	70.9	14.1	104.5	77.2	87.0	86.0	6.16	4.5	7052
W-Unin/40-C/1	2.79	11.1	2.05	0.96	47.7	23.7	56.2	48.2	44.9	80.4	3.50	4.6	3431
W-SR1200/40-C/1	1.43	8.4	4.07	1.36	66.9	15.6	93.9	65.0	82.6	93.7	6.04	4.6	7010
W-SR55/40-C/1	5.45	26.7	0.79	0.73	54.0	66.8	56.0	81.6	54.6	85.0	1.28	5.0	2758
W-NB/15-C/2	2.23	14.1	2.79	1.65	93.6	32.0	109.5	68.8	87.6	74.6	2.32	8.8	5731

explained by the input parameters for estimating the behaviour of the connection; in the experimental results, the CV obtained for the elastic stiffness $k_{con,el}$ of the connections was very high in some cases, e.g. almost 60% for uninsulated specimens in the shear direction. Nevertheless, the analytical model better estimated plastic stiffness; on average $k_{40\text{-}90}$ was overestimated by 2%, with a 15% CV.

The ultimate deformation capacity, δ_u, is on average 7% higher according to the analytical model than that obtained from the experimental tests, but with a higher scatter of results (tests in which the load-bearing capacity was not obtained in both loading directions are excluded from the statistics). Due to the overestimation of the ultimate displacement capacity, the ductility, μ, and total potential energy, E_{INP}, are also overestimated. It can be seen, however, that the overestimation is significantly higher for μ (the results of the experimental tests are overestimated by 27% with a CV equal to 20%). The higher error in the calculation of μ originates from overestimation of both the stiffness and ultimate displacement, δ_u, while the 12% overestimation of E_{INP} is prevailingly the result of the overestimation of δ_u. If the potential energy is re-evaluated up to the ultimate displacements achieved in the experimental tests (denoted by $E_{INP}^{(red)}$ in Table 4), the analytical curves prove to be very good approximations of the experimental curves, with the relative difference in potential energy between them being just 1% on average, with a satisfactory 6% CV.

5.2. Influence of insulation

Since the insulated specimens were only tested up to a vertical load of 50 kN/m, a direct comparison of experimental results between the insulated and uninsulated specimens is only possible for the specimens with a vertical load level of 10 kN/m. As seen from Fig. 7 and the test results in Table 3, the bedding insulation does not seem to significantly change the lateral load-bearing capacity (H_{max}) of the system. Specifically, the load-bearing capacity of the W-NB/15-C/1 specimen with Flex.ins. was 8% higher in the experimental tests compared to the corresponding uninsulated specimen. According to the analytical model, H_{max} should be approximately 1% higher in this specimen (see Fig. 9). In specimen W-SR55/15-C/1 the limit displacement of the experimental test set-up was reached before its maximum load-bearing capacity could be obtained; nevertheless, its maximum resistance, at 100 mm shear displacement, was similar (3% higher) to the load-bearing capacity of the uninsulated specimen, whereas according to the analytical model the difference should be less than 0.5%. For the insulated specimen W-SR55/40-C/1 (b_e = 400 mm) the average experimental lateral load-bearing capacity obtained was very similar as for the uninsulated W-Unin/40-C/1 - where again the load-bearing capacity of the W-SR55/40-C/1 was not reached but should, according to the analytical model, be approximately 7% lower than the uninsulated specimen.

More important than the relatively small changes in lateral load-bearing capacity of the insulated specimens, as proven by experimental tests as well as suggested by the analytical model, is the reduction in stiffness brought by the bedding insulation, resulting from additional rotations of the walls due to deformation of the insulation under horizontal loading. This influence is evident in Fig. 10, where the secant stiffness obtained at amplitude displacements in the first loading cycles is presented for all walls with an angle bracket edge distance, b_e, of 150 mm. For specimens under low vertical load, both experimental tests as well as analytical models showed a 60% reduction in elastic stiffness, k_{el}, when b_e was equal to 150 mm (W-SR55/15-C/1, W-NB/15-C/1). The load-bearing capacity of an insulated specimen with an increased edge distance (b_e equal to 400 mm, W-SR55/40-C/1) was 61% lower than an uninsulated specimen according to experimental tests, and 68% lower according to the analytical model. Under a higher vertical load a 41% decrease in k_{el} was observed in a wall containing Flex. ins in comparison to a wall containing Stiff.ins (compared to a 49% drop according to the analytical model).

Though the insertion of insulation provides higher ultimate lateral displacements of the walls (on average 28% higher for W-SR55/15-C/1 and W-NB/15-C/1 compared to the uninsulated walls, and predicted to be 27% higher according to the analytical model), the insulation causes a reduction in ductility overall due to a significantly large decrease in stiffness.

5.3. Influence of vertical load

Although conducted on only a small number of samples, the results of the experimental tests confirm that the vertical load has a positive influence on the lateral load-bearing capacity, primarily as a result of the increase in frictional forces. In the case of the uninsulated specimen the lateral load-bearing capacity increased by more than 130% (150% analytically) when the vertical load was raised from 10 to 100 kN/m. In the case of the insulated specimens (W-NB/15-C/1 vs. W-NB/15-C/2) an increase in vertical load from 10 to 50 kN/m resulted in an increase in load-bearing capacity of approximately 70% (compared to almost 90% analytically). It should be noted that the experimental test on W-NB/15-C/2 was conducted under a different loading rate, which influences the response [49], but the influence is not significant given the relative changes observed with respect to the different vertical loads applied.

At a higher vertical load the stiffness increased in both the uninsulated (as also found in Refs. [38,50,51]) and insulated specimens. In the experimental tests, the higher vertical loads mentioned resulted in an increase in elastic stiffness, k_{el}, of 340% in uninsulated walls and 100% in insulated walls. The increase in stiffness can be attributed to frictional forces caused by the increased compressive stress at the wall-to-slab interface, and the consequent delay in rocking (obtained at higher forces relative to H_{max}). The increase in compressive stresses (beyond the elastic limit) also causes the CLT wall panel to embed into the CLT slab prior to the onset of rocking, which in the end represents 4% of the total ultimate lateral displacement for the uninsulated specimen (W-Unin/15-C/2). Local embedment into the slab at the edge of the CLT wall was also observed in the case of the insulated specimens (the analytical contribution to lateral deformations can be seen in Fig. 9). Nevertheless, due to higher lateral loads, the bending and shear
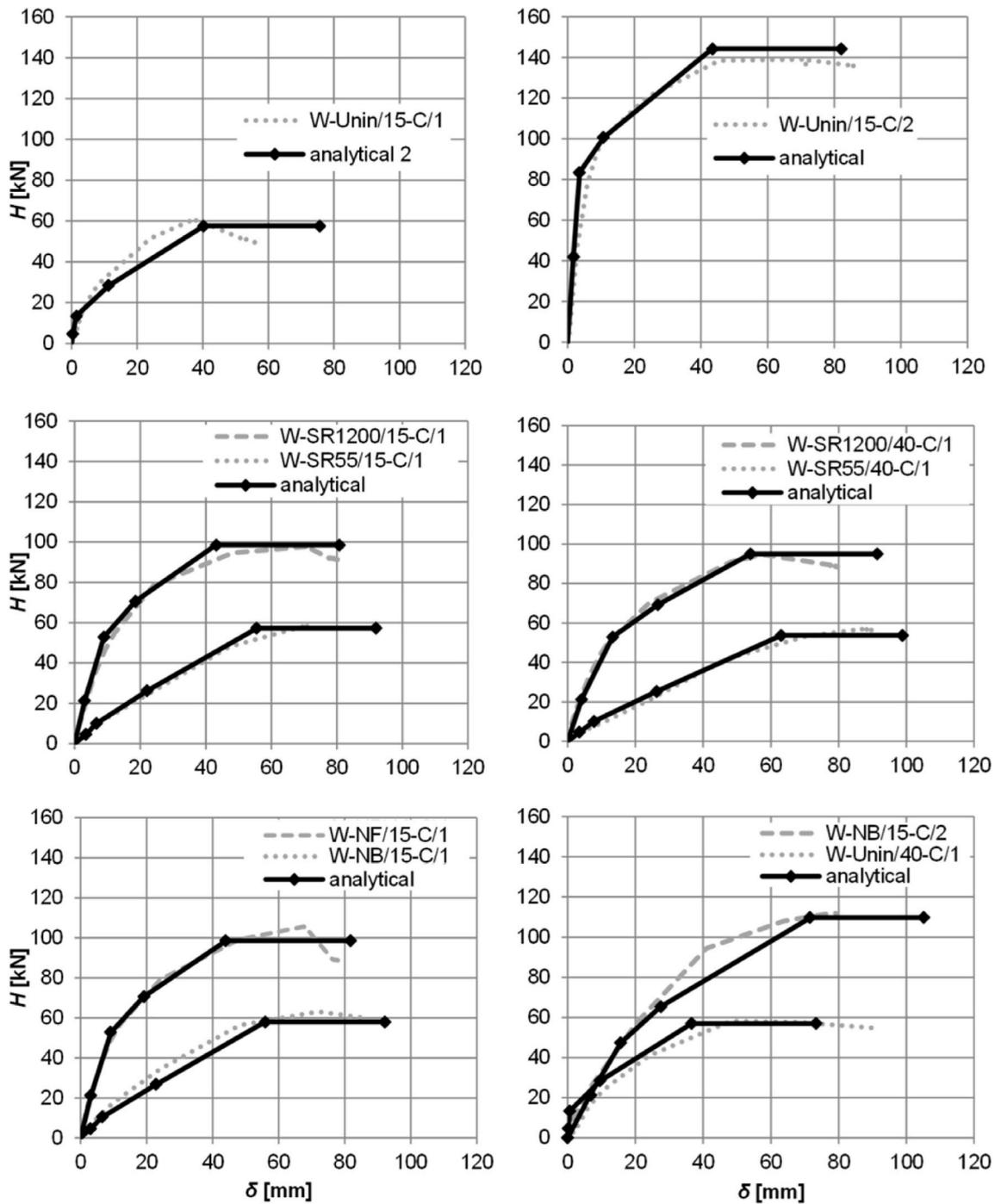
Fig. 8. Analytical multi-linear lateral response prediction compared to the experimental backbone curves.

deformations of the CLT wall panel also increase, e.g. under a 100 kN/m vertical load the latter accounts for 12% of the total lateral deformation in the uninsulated wall (see Fig. 9).

The experimental tests proved a 23% increase in ultimate displacement in the uninsulated wall at a higher vertical load (100 kN/m compared to 10 kN/m), while the analytical model foresees a 14% increase. In the insulated walls, W-NB, a change in vertical load from 10 kN/m to 50 kN/m should, according to the analytical prediction, also result in a 14% increase in the ultimate displacement, but in fact in the experimental tests lower ultimate displacements were observed under a higher vertical load.

6. Summary and conclusions

Experimental cyclic shear tests on full-size CLT walls were conducted in order to study the response of CLT wall specimens with insulated steel angle bracket connections under lateral force, when founded on CLT slabs with or without a sound insulation layer and subjected to different vertical loads. By comparing experimental results the influence of the sound insulation layer and the level of vertical load was evaluated. Furthermore, an analytical model was proposed to predict the multi-linear lateral load-displacement response, which can be used for in-depth analysis of the lateral response of the walls tested and further applications. The analytical model was verified by comparing the estimated results to those experimentally obtained.
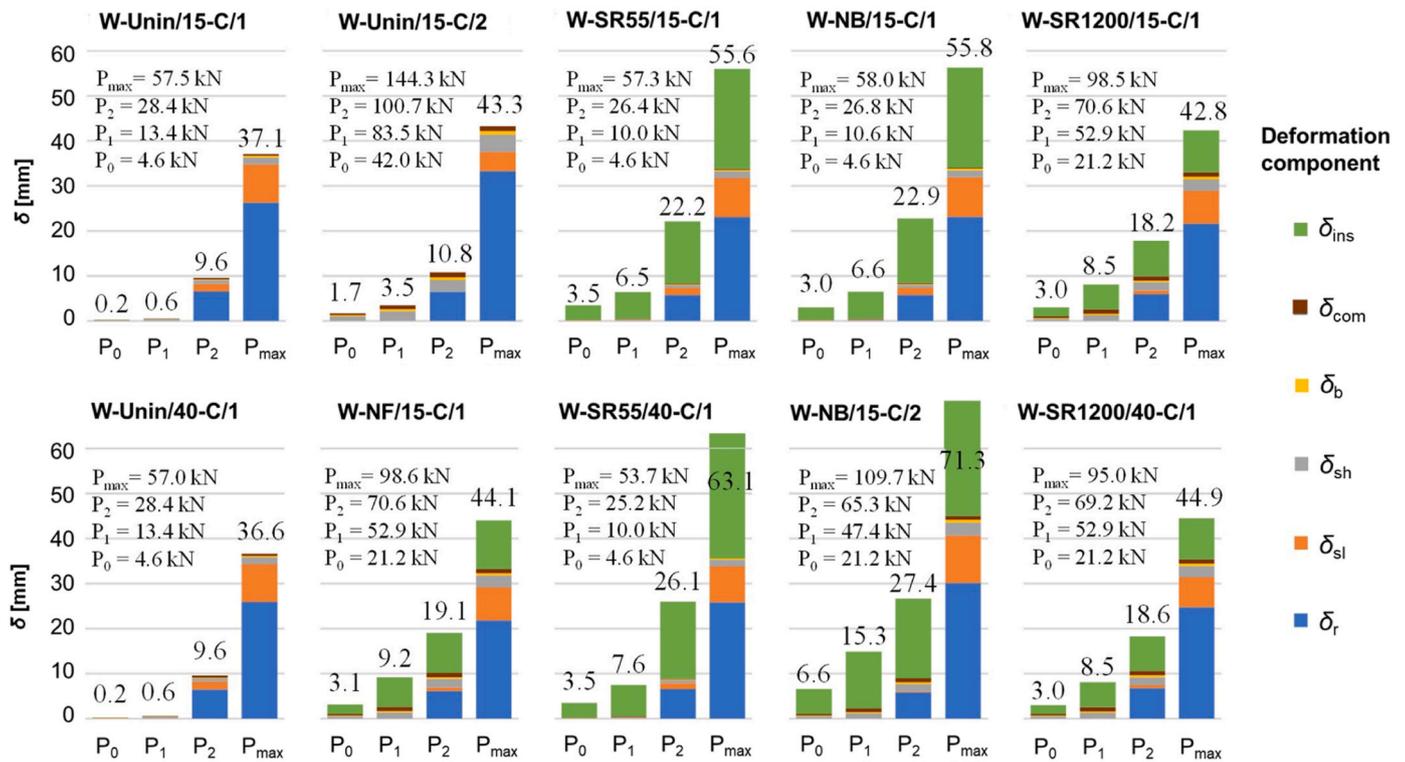
Fig. 9. Analytically determined total lateral displacements (δ) for all walls by limit point, with the contributions of individual components depicted in different colours and the lateral resistances evaluated. (For interpretation of the references to colour in this figure legend, the reader is referred to the Web version of this article.)

Table 4
Ratio of analytical to experimental results (average of both directions of loading considered for the experimental results).

Test	Analytical/Experimental							
	k_{el}	k_{40-90}	H_{max}	δ_u	μ	$\mu^{(red)}$	E_{INP}	$E_{INP}^{(red)}$
W-Unin/15-M/1	0.74	0.89	0.88	1.18	0.97	0.82	1.15	0.94
W-Unin/15-C/1	0.91	0.95	0.98	<u>1.16</u>	<u>1.14</u>	0.98	<u>1.26</u>	1.04
W-Unin/15-C/2	1.73	0.84	1.03*	1.07	1.91	1.78	1.13	1.04
W-SR55/15-C/1	1.09	1.06	0.95*	1.28	1.41	1.11	1.43	1.00
W-NB/15-C/1	0.80	0.99	0.91	<u>1.08**</u>	<u>0.84</u>	0.78	<u>1.01</u>	0.91
W-SR1200/15-C/1	1.26	1.08	1.00	<u>0.96</u>	<u>1.28</u>	1.28	<u>1.01</u>	1.01
W–NF/15-C/1	1.19	1.17	0.94*	0.95	1.15	1.15	0.95	0.95
W-Unin/40-C/1	1.40	1.18	1.01	<u>0.91**</u>	<u>1.45</u>	1.45	<u>1.00</u>	1.00
W-SR1200/40-C/1	1.47	1.19	1.01	<u>0.88**</u>	<u>1.39</u>	1.39	<u>0.94</u>	0.94
W-SR55/40-C/1	1.16	1.07	0.96*	1.16	1.39	1.20	1.36	1.09
W-NB/15-C/2	1.07	0.72	1.00	<u>1.41**</u>	<u>1.53</u>	1.08	<u>1.50</u>	0.91
Average	1.21	1.02	0.98	1.07	1.27	1.22	1.12	0.99
(CV)	(0.23)	(0.15)	(0.04)	(0.18)	(0.20)	(0.23)	(0.18)	(0.06)

Note: Only cyclic tests are considered for the calculation of average and CV values. In tests where H_{max} is denoted by * the load-bearing capacity and ultimate deformation were not achieved in both directions. In tests where δ_u is denoted by ** the 20% drop in load-bearing capacity was not obtained. The average δ_u, μ and E_{INP} presented in the table are calculated considering only the values underlined (i.e. tests where load-bearing capacity was achieved in both directions).

The following conclusions can be drawn from the study:

- The experimental tests confirmed that the angle brackets used for the connections are able to provide substantial load-bearing capacity in both the shear and tensile (uplift) directions [9], allowing significant lateral deformations in the wall (2.5% drift in the uninsulated wall, and more than 3% in the insulated walls).
- The insulation layer under the wall led to only minor changes in the load-bearing capacity of the walls under lower vertical loads; on average a 4% increase was obtained in the experimental tests, while an average overall decrease of 2% should be obtained for the variations tested according to the analytical model. On the other hand, the stiffness of the wall is significantly reduced, due to additional

lateral deformation of the wall, enabled by deformation of the insulation. The elastic stiffness decreased to less than 40% that of the uninsulated wall in the case of the more flexible insulation at a low vertical load.

- The presence of vertical load has several effects on the shear response of the CLT wall. Experiments confirmed that a higher vertical load substantially increases the load bearing capacity, as well as the stiffness of the shear wall, due to the associated increase in friction, the relatively higher forces at the onset of the rocking mechanism (the CLT wall system is more resistant to shear deformations), and deformations due to the embedment of the CLT wall panel into the CLT slab. In the wall system analysed it was shown that the lateral
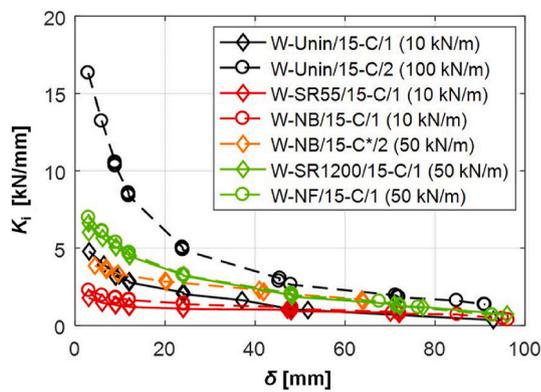
Fig. 10. Secant stiffness for positive amplitude displacement loading cycles in uninsulated and insulated specimens under different vertical loads (edge position of the angle brackets, b_e, equal to 150 mm).

load-bearing capacity of the uninsulated wall increased by more than 130% when the vertical load was raised from 10 to 100 kN/m.

- The analytical model proposed proved to estimate the load-bearing capacity and plastic stiffness with adequate accuracy and achieved acceptable approximation to the experimental curves in terms of potential energy, even though the elastic stiffness is, in general, overestimated. What could be an issue, however, is overestimation of the ultimate displacement capacity - by 7% on average but with a high CV. Additional experimental tests are needed to analyse whether this overestimation arises from the model itself, or from the input parameters, in particular from the connections.
- The test results presented and the analytical model proposed may form the basis for further research in order to determine the behaviour factor (q-factor) for the seismic design of timber structures with bedding insulation. Due to reduced ductility, the q-factor values defined in the codes for seismic design should most likely be reduced. This should, however, be confirmed by additional in-depth studies on this topic, since a less stiff response of the CLT wall system and higher displacement capacities were also obtained.
- The analytical model offers an in-depth understanding of the behaviour of insulated CLT walls under lateral loading and a possibility to simplify the finite element modelling and design of CLT structures.

Ethical approval

The authors declare that there is no issue concerning ethical standards.

Informed consent

Informed consent was obtained from all individual participants included in the study.

CRediT authorship contribution statement

Boris Azinović: Writing – original draft, Methodology, Formal analysis, Visualization, Validation. **Tomaž Pazlar:** Conceptualization, Investigation, Supervision. **Meta Kržan:** Investigation, Formal analysis, Writing – review & editing, Validation.

Declaration of competing interest

The authors declare that they have no known competing financial interests or personal relationships that could have appeared to influence the work reported in this paper.

Acknowledgements

Appendix A. Supplementary data

Supplementary data to this article can be found online at https://doi.org/10.1016/j.jobe.2021.103183.

References

[1] R. Brandner, G. Flatscher, A. Ringhofer, G. Schickhofer, A. Thiel, Cross laminated timber (CLT): overview and development, Eur. J. Wood Wood Prod. 74 (2016) 331–351.

[2] R.M. Foster, T.P.S. Reynolds, M.H. Ramage, Proposal for defining a tall timber building, J. Struct. Eng. 142 (2016), 02516001, https://doi.org/10.1061/(ASCE)ST.1943-541X.0001615.

[3] M.H. Ramage, H. Burridge, M. Busse-Wicher, G. Fereday, T. Reynolds, D.U. Shah, G. Wu, L. Yu, P. Fleming, D. Densley-Tingley, J. Allwood, P. Dupree, P.F. Linden, O. Scherman, The wood from the trees: the use of timber in construction, Renew. Sustain. Energy Rev. 68 (2017) 333–359.

[4] S. Pei, J.W. van de Lindt, Seismic numerical modeling of a six-story light-frame wood building: comparison with experiments, J. Earthq. Eng. 15 (2011) 924–941.

[5] M. Izzi, D. Casagrande, S. Bezzi, D. Pasca, M. Follesa, R. Tomasi, Seismic behaviour of Cross-Laminated Timber structures: a state-of-the-art review, Eng. Struct. 170 (2018) 42–52, https://doi.org/10.1016/j.engstruct.2018.05.060.

[6] M. Fragiacomo, B. Dujić, I. Šušteršič, Elastic and ductile design of multi-storey crosslam massive wooden buildings under seismic actions, Eng. Struct. 33 (2011) 3043–3053.

[7] T. Reynolds, D. Casagrande, R. Tomasi, Comparison of multi-storey cross-laminated timber and timber frame buildings by in situ modal analysis, Construct. Build. Mater. 102 (2016) 1009–1017, https://doi.org/10.1016/j.conbuildmat.2015.09.056.

[8] H. Reichelt, U. Gerhaher, S. Wiederin, R. Maderebner, Characteristics of acoustic layers for structural design of timber constructions, in: Proc. WCTE 2016 World Conf. Timber Eng., TUVerlag, Vienna, Austria, 2016, pp. 2904–2911.

[9] M. Kržan, B. Azinović, Cyclic response of insulated steel angle brackets used for cross-laminated timber connections, Eur. J. Wood Wood Prod. 79 (2021) 691–705.

[10] Pitzl, getzner GmbH, GePi connectors: powerful soundproofing angle brackets. https://www.pitzl-connectors.com/gepi/, 2018.

[11] Y. Shen, J. Schneider, S. Tesfamariam, S.F. Stiemer, Z. Chen, Cyclic behavior of bracket connections for cross-laminated timber (CLT): assessment and comparison of experimental and numerical models studies, J. Build. Eng. 39 (2021) 102197.

[12] I. Gavric, M. Fragiacomo, A. Ceccotti, Cyclic behaviour of typical metal connectors for cross-laminated (CLT) structures, Mater. Struct. 48 (2015) 1841–1857.

[13] G. D'Arenzo, G. Rinaldin, M. Fossetti, M. Fragiacomo, F. Nebiolo, M. Chiodega, Tensile and shear behaviour of an innovative angle bracket for CLT structures, in: Proc. WCTE 2018, Seoul, South Korea, 2018.

[14] G. D'Arenzo, G. Rinaldin, M. Fossetti, M. Fragiacomo, An innovative shear-tension angle bracket for Cross-Laminated Timber structures: experimental tests and numerical modelling, Eng. Struct. 197 (2019) 109434.

[15] L. Pozza, A. Saetta, M. Savoia, D. Talledo, Coupled axial-shear numerical model for CLT connections, Construct. Build. Mater. 150 (2017) 568–582.

[16] J. Liu, F. Lam, Experimental test of coupling effect on CLT angle bracket connections, Eng. Struct. 171 (2018) 862–873.

[17] J. Liu, F. Lam, R.O. Foschi, M. Li, Modeling the coupling effect of CLT connections under biaxial loading, J. Struct. Eng. 146 (2020).

[18] I. Gavric, M. Fragiacomo, A. Ceccotti, Cyclic behavior of CLT wall systems: experimental tests and analytical prediction models, J. Struct. Eng. 141 (2015), 04015034.

[19] D. Casagrande, S. Rossi, T. Sartori, R. Tomasi, Proposal of an analytical procedure and a simplified numerical model for elastic response of single-storey timber shear-walls, Construct. Build. Mater. 102 (2016) 1101–1112, https://doi.org/10.1016/j.conbuildmat.2014.12.114.

[20] D. Casagrande, G. Doudak, L. Mauro, A. Polastri, Analytical approach to establishing the elastic behavior of multipanel CLT shear walls subjected to lateral loads, J. Struct. Eng. 144 (2018), 04017193, https://doi.org/10.1061/(ASCE)ST.1943-541X.0001948.

[21] V. Nolet, D. Casagrande, G. Doudak, Multipanel CLT shearwalls: an analytical methodology to predict the elastic-plastic behaviour, Eng. Struct. 179 (2019) 640–654, https://doi.org/10.1016/j.engstruct.2018.11.017.

[22] M. Masroor, G. Doudak, D. Casagrande, The effect of bi-axial behaviour of mechanical anchors on the lateral response of multi-panel CLT shearwalls, Eng. Struct. 224 (2020) 111202, https://doi.org/10.1016/j.engstruct.2020.111202.

[23] Y.L. Shen, J. Schneider, S. Tesfamariam, S.F. Stiemer, Z.G. Mu, Hysteresis behavior of bracket connection in cross-laminated-timber shear walls, Construct. Build. Mater. 48 (2013) 980–991.

[24] F. Benedetti, V. Rosales, A. Opazo-Vega, J. Norambuena-Contreras, A. Jara-Cisterna, Experimental and numerical evaluation of hold-down connections on radiata pine Cross-Laminated-Timber shear walls: a case study in Chile, Eur. J. Wood Wood Prod. 77 (2019) 79–92.

[25] M. Shahnewaz, S. Alam, T. Tannert, In-plane strength and stiffness of cross-laminated timber shear walls, Buildings 8 (2018) 100.

[26] V. Awad, L. Giresini, M. Koshihara, M.L. Puppio, M. Sassu, Experimental analyses and numerical models of CLT shear walls under cyclic loading, in: G. Concu (Ed.), Wood Civ. Eng., InTech, 2017, https://doi.org/10.5772/65024.

[27] M.A. Kovacs, L. Wiebe, Controlled rocking CLT walls for buildings in regions of moderate seismicity: design procedure and numerical collapse assessment, J. Earthq. Eng. 23 (2019) 750–770, https://doi.org/10.1080/13632469.2017.1326421.

[28] C. Demirci, C. Málaga-Chuquitaype, L. Macorini, Seismic shear and acceleration demands in multi-storey cross-laminated timber buildings, Eng. Struct. 198 (2019) 109467, https://doi.org/10.1016/j.engstruct.2019.109467.

[29] A. Polastri, M. Izzi, L. Pozza, C. Loss, I. Smith, Seismic analysis of multi-storey timber buildings braced with a CLT core and perimeter shear-walls, Bull. Earthq. Eng. 17 (2019) 1009–1028, https://doi.org/10.1007/s10518-018-0467-9.

[30] G. Rinaldin, C. Amadio, M. Fragiacomo, A component approach for the hysteretic behaviour of connections in cross-laminated wooden structures, Earthq. Eng. Struct. Dyn. 42 (2013) 2023–2042, https://doi.org/10.1002/eqe.2310.

[31] L. Franco, L. Pozza, A. Saetta, M. Savoia, D. Talledo, Strategies for structural modelling of CLT panels under cyclic loading conditions, Eng. Struct. 198 (2019) 109476, https://doi.org/10.1016/j.engstruct.2019.109476.

[32] J.W. van de Lindt, M.O. Amini, D. Rammer, P. Line, S. Pei, M. Popovski, Seismic performance factors for cross-laminated timber shear wall systems in the United States, J. Struct. Eng. 146 (2020), 04020172, https://doi.org/10.1061/(ASCE)ST.1943-541X.0002718.

[33] W. Seim, J. Hummel, T. Vogt, Earthquake design of timber structures – remarks on force-based design procedures for different wall systems, Eng. Struct. 76 (2014) 124–137, https://doi.org/10.1016/j.engstruct.2014.06.037.

[34] D. Casagrande, G. Doudak, A. Polastri, A proposal for the capacity-design at wall- and building-level in light-frame and cross-laminated timber buildings, Bull.

[35] G. Schickhofer, A. Ringhofer, The Seismic Behaviour of Buildings Erected in Solid Timber Construction-Seismic Design According to EN 1998 for a 5-storey Reference Building in CLT, Graz University of Technology, Graz, Austria, 2012.

[36] G. Tamagnone, G. Rinaldin, M. Fragiacomo, A novel method for non-linear design of CLT wall systems, Eng. Struct. 167 (2018) 760–771, https://doi.org/10.1016/j.engstruct.2017.09.010.

[37] A. Sandoli, C. D'Ambra, C. Ceraldi, B. Calderoni, A. Prota, Role of perpendicular to grain compression properties on the seismic behaviour of CLT walls, J. Build. Eng. (2020) 101889, https://doi.org/10.1016/j.jobe.2020.101889.

[38] J. Hummel, G. Flatscher, W. Seim, G. Schickhofer, CLT wall elements under cyclic loading - details for anchorage and connection, in: COST Action FP1004, 2013, pp. 152–165.

[39] OIB, ETA 14-0349, 2020.

[40] DIBt, ETA 11-0284, 2019.

[41] Getzner, Intelligent sound insulation solutions in wood construction. https://www.getzner.com/en/applications/construction/building-acoustics/resilient-bedding-of-elements-in-timber-construction, 2018. (Accessed 1 February 2019).

[42] ISO 16670:2003, Timber Structures - Joints Made with Mechanical Fasteners - Quasi-Static Reversed-Cyclic Test Method, ISO, 2003.

[43] EN 12512:2005, Timber Structures - Test Methods - Cyclic Testing of Joints Made with Mechanical Fasteners, CEN, 2005.

[44] J. Hummel, W. Seim, S. Otto, Steifigkeit und Eigenfrequenzen im mehrgeschossigen Holzbau, Bautechnik 93 (2016) 781–794.

[45] M. Wallner-Novak, M. Augustin, J. Koppelhuber, K. Pock, Cross-Laminated Timber Structural Design, vol. 2, Applications, ProHolz Austria, 2018.

[46] A.J.M. Leijten, The bearing strength capacity perpendicular to grain of Norway spruce–Evaluation of three structural timber design models, Construct. Build. Mater. 105 (2016) 528–535.

[47] T. Claus, W. Seim, J. Liese, Friction under cyclic loading, in: Proc. WCTE 2018–World Conf. Timber Eng. Seoul, 2018.

[48] J.P. Almeida, K. Beyer, R. Brunner, T. Wenk, Characterization of mortar–timber and timber–timber cyclic friction in timber floor connections of masonry buildings, Mater. Struct. 53 (2020) 1–14.

[49] B. Azinović, M. Kržan, T. Pazlar, In-plane lateral testing of timber based shear walls and the influence of loading rate, in: 1CroCEE, Zagreb, Croatia, 2021, https://doi.org/10.5592/CO/1CroCEE.2021.92.

[50] G. Flatscher, K. Bratulic, G. Schickhofer, Experimental tests on cross-laminated timber joints and walls, Proc. Inst. Civ. Eng. - Struct. Build. 168 (2015) 868–877, https://doi.org/10.1680/stbu.13.00085.

[51] M. Popovski, J. Schneider, M. Schweinsteiger, Lateral load resistance of cross-laminated wood panels, in: World Conf. Timber Eng, 2010, pp. 20–24.